Original Article

Differentiation of inflammatory pseudotumors and malignant pulmonary nodules using the time-to-peak in first-pass dual-input volume computed tomography-perfusion

Chengwei Guo[1], Xiaobo Zhang[2], Sandi Shen[3], Weijun Chen[1], Xuejing Wang[1], Liang Zhao[1], Shuqing Han[4]

[1]Department of Radiology, No. 82 Group Hospital of Chinese People's Liberation Army, Baoding, China; [2]Department of Radiology, the First Medical Centre, Chinese People's Liberation Army General Hospital, Beijing, China; [3]Thoracic Surgery, The Sixth Affiliated Hospital of Guangzhou Medical University, Qingyuan People's Hospital, Qingyuan, China; [4]Department of Pathology, No. 82 Group Hospital of Chinese People's Liberation Army, Baoding, China

Contributions: (I) Conception and design: C Guo; (II) Administrative support: C Guo, W Chen; (III) Provision of study materials or patients: C Guo, X Zhang, S Shen; (IV) Collection and assembly of data: C Guo, X Wang, L Zhao; (V) Data analysis and interpretation: C Guo, X Wang, L Zhao, S Han; (VI) Manuscript writing: All authors; (VII) Final approval of manuscript: All authors.

Correspondence to: Chengwei Guo, MD. Department of Radiology, No. 82 Group Hospital of Chinese People's Liberation Army, 991, East Baihua Road, Baoding 071000, China. Email: gcw323765@163.com.

Background: Inflammatory pseudotumors (IPTs) are often misdiagnosed as malignant solitary pulmonary nodules (SPNs) because their imaging features overlap with those of malignant SPNs, leading to overtreatment. The purpose of this article was to investigate the value of first-pass enhanced time-to-peak (TTP) in distinguishing IPTs from malignant SPNs using dual-input volume computed tomography perfusion (DI-CTP).

Methods: This retrospective study included consecutive patients from No. 82 Group Hospital of Chinese People's Liberation Army with IPTs or malignant SPNs by surgery or biopsy from June 2016 to October 2021. Pulmonary artery flow (PF), bronchial artery flow (BF), perfusion index (PI), time-density curve, total perfusion (TLP), and first-pass TTP for all SPNs were determined by DI-CTP. The receiver operating characteristic (ROC) curve was used to analyse the values of TTP and other perfusion parameters in the differential diagnosis of IPTs and malignant SPNs.

Results: Ninety-eight patients were enrolled, including 25 with IPTs and 73 with malignant SPNs. The intraclass correlation coefficient (ICC) for inter-observer and intra-observer reliability of all parameters was perfect (all ICCs >0.90, P<0.01). Compared with IPTs, the malignant SPNs showed significantly higher PF, TLP, and TTP (all P<0.01), without significant differences in BF and PI (all P>0.05). The area under the curve of TTP was 0.987, which was higher than those of the other perfusion parameters (0.987 *vs.* 0.752 *vs.* 0.609 *vs.* 0.728 *vs.* 0.628). With a cut-off TTP of 18.10 s to distinguish IPNs from malignant SPNs, the sensitivity, specificity, positive predictive value, negative predictive value, and accuracy were 92.0%, 97.3%, 97.3%, 96.0%, and 96.9%, respectively. The sensitivity, specificity, and accuracy of CT plain scan combined with DI-CTP in diagnosing pulmonary nodules were 100%, 96.83%, and 98.97%, respectively.

Conclusions: Compared with other perfusion parameters, TTP may be a more valuable parameter to differentiate IPTs from malignant SPNs.

Keywords: Computed tomography (CT); perfusion imaging; lung neoplasms; receiver operating characteristic curve (ROC curve); inflammatory pseudotumor

Submitted Jun 22, 2024. Accepted for publication Mar 03, 2025. Published online Mar 28, 2025.
doi: 10.21037/qims-24-1261
View this article at: https://dx.doi.org/10.21037/qims-24-1261

Introduction

The solitary pulmonary nodule (SPN) is a common imaging sign, whose detection rates are gradually increasing due to advances in imaging technology and improved awareness of physical examination. Adenocarcinoma and squamous cell carcinoma account for approximately 75% of all malignant SPNs (1-3). The lung is the second simultaneous organ for pulmonary metastasis, and almost one-third of cancer deaths involve lung metastasis (1). The inflammatory pseudotumor (IPT) is an inflammatory, proliferative tumor-like nodule, and a rare benign SPN in the lung (4). IPTs are often misdiagnosed as malignant SPNs and overtreated with procedures such as surgical resection and puncture biopsy since their imaging features overlap with those of malignant SPNs (5-11). However, biopsy is an invasive procedure that carries the risk of pneumothorax, bleeding, and even tumor metastasis (12). Therefore, a non-invasive method to differentiate between IPTs and malignant SPNs is needed to avoid overtreatment of IPTs.

In recent years, the advent of dual-input volume computed tomography (CT) perfusion (DI-CTP) allowed the differential diagnosis of pulmonary nodules. Previous studies have demonstrated that lung tumors have a dual blood supply by the pulmonary and aortic systems (13,14). The dual vascular supply of lung tumors can be quantitated with DI-CTP perfusion parameters, and dynamic first-pass enhanced CT perfusion volume data can be obtained (13,15-17). Indeed, Yuan *et al.* (13) found that compared with malignant SPNs, benign SPNs had significantly higher pulmonary artery flow (PF) and perfusion index (PI), and bronchial artery flow (BF) was significantly lower. Meanwhile, PI had the highest diagnostic efficiency in differentiating between benign and malignant pulmonary nodules, with a sensitivity of 95% and a specificity of 83%. In addition, Bohlsen *et al.* (18) reported that malignant lesions showed statistically significantly higher PF than benign lesions, with no significant differences in BF and PI between malignant and benign lesions. Malignant tumors often invade the pulmonary artery of the affected lung segment, causing pulmonary artery stenosis or occlusion. With its aggravation, hyperplasia of fibers induces the obstruction of the pulmonary artery, and bronchial arteries supplement blood supply to the ischemic lung tissue (19,20). Therefore, a new parameter is needed to effectively differentiate between benign and malignant SPNs.

The time-to-peak (TTP) derived from time-density curve (TDC) reflects the features of the dominant blood supply in pulmonary nodules, which is physiologically based on dual blood supply in the lung (15). Previous studies applying contrast-enhanced ultrasound or 64-detector row CT systems have reported lower TTP in benign SPNs compared with malignant SPNs (21,22). Currently, studies using TTP to differentiate between IPTs and malignant SPNs are scarce, especially those examining different subtypes of malignant SPNs, based on the 320-detector row CT system.

Therefore, this study aimed to investigate the value of DI-CTP for differentiating between IPTs and malignant SPNs using TTP and direct visualization of the TDC. We present this article in accordance with the STARD reporting checklist (available at https://qims.amegroups.com/article/view/10.21037/qims-24-1261/rc).

Methods

Study population

This study included consecutive patients from No. 82 Group Hospital of Chinese People's Liberation Army who underwent surgery or biopsy from June 2016 to October 2021 to confirm the nature of SPNs. This retrospective study was approved by the ethics committee of No. 82 Group Hospital of Chinese People's Liberation Army (No. 2021011) and conducted in accordance with the Declaration of Helsinki (as revised in 2013). The requirement of informed consent was waived due to the retrospective nature of the study.

Inclusion criteria were: (I) SPNs manifesting as solid pulmonary nodules with a diameter of 1–3 cm; (II) pathologically confirmed IPTs or malignant lesions (squamous cell carcinoma, adenocarcinoma, or lung metastases) within 2 weeks after DI-CTP; (III) solitary lesions. Exclusion criteria were: (I) ground glass nodules (GGNs) or subsolid nodules (solid content ≤50%); (II) merged mediastinal and hilar enlarged lymph nodes (diameter ≥1.5 cm); (III) respiratory dysfunction; (IV) previous reactions to iodinated contrast media; or (V) poor image quality or impossible body registration; (VI) patients with a confirmed history of primary pulmonary nodules.

CT perfusion imaging technique

Per routine practice, all patients were informed of radiation exposure and potential harm. The radiation dose was calculated from the dose-length product (DLP) listed in the

exposure summary sheet generated by the CT system and multiplied by a k-factor of 0.014.

Before examination, all patients underwent breathing training to ensure they could hold their breath for the entire perfusion procedure (i.e., 34 s). DI-CTP was performed using a 320-detector row CT scanner (Aquilion ONE, Canon Medical Systems, Japan). Before perfusion CT, plain scan localization was performed, and the 16-cm coverage included the nodule, pulmonary artery trunk, left atrium, and thoracic aorta. The contrast medium (CM) dose (350 mg I/mL) was adjusted according to patient weight: at least 30 mL for patients ≤60 kg and 0.5 mL/kg for patients >60 kg (maximum of 50 mL). The CM was injected with a dual-head power injector (Ulrich Medical, Ulm, Germany) at a rate of 6 mL/s via a 20-G intravenous catheter placed in the antecubital vein, followed by a 20 mL saline flush at the same injection rate. Two seconds after starting the bolus injection, 17 intermittent low-dose volume acquisitions were made at 2-s intervals with no table movement. The dual-input CT imaging was performed with the following parameters: tube voltage, 100 kV; tube current, 30 mA; gantry rotation speed, 0.5 s; slice thickness, 0.5 mm; reconstruction layer thickness, 0.5 mm. The total scanning time was 34 s. The data were processed with adaptive iterative dose reduction (AIDR 3D) and automatically reconstructed with 320 images per volume and a total of 5,440 images for the entire volume perfusion data set.

Data post-processing and image analysis

The dual-input maximum slope analysis method was used to process the perfusion volume data. Volume registration was performed and loaded into the body perfusion analysis software to reduce misregistration respiratory artifacts and facilitate the evaluation of perfusion CT datasets (13). Two radiologists (Observer 1 and Observer 2, with 5 and 10 years of experience in lung DI-CTP, respectively) measured the parameters independently using operator-defined regions of interest (ROIs). Both radiologists were blinded to the clinical characteristics of the patients. In order to ensure the consistency of the ROIs, a freehand ROI based on the slices of the entire lesion was drawn manually along the edge of the nodule, avoiding visible blood vessels, lung tissue, necrotic liquefaction areas, cavities, calcifications, fat density, and artifacts and the TDC was generated for the contrast medium first-pass attenuation in the SPN. PF, BF, PI (PI = PF/PF + BF), and TDC were obtained by DI-CTP. Total perfusion (TLP, TLP = PF + BF) was calculated. The first-pass TTP obtained from the TDC was measured.

The averages of the measurements from three ROIs were calculated for each parameter. In order to assess the intra-observer agreement, these parameters were measured twice by Observer 1 (2 weeks apart). In order to assess the inter-observer agreement, the averages of parameters measured twice by Observer 1 were compared with those measured once by Observer 2.

Statistical analysis

All statistical analyses were performed using SPSS 27.0 (Chicago, IL, USA) and MedCalc software (Mariakerke, Belgium). Intra-observer and inter-observer agreements were evaluated using intraclass correlation coefficients (ICCs), and Bland-Altman plots with 95% limits of agreement were used. ICC <0.40, 0.40–0.75, >0.75 indicated poor, fair-to-good, and excellent agreement. The correlation between each index's first and second measurements was also assessed using Pearson's correlation. The coefficients of variation (CVs) were calculated, and the target CV was <20% (23). Assessment of PI with scattered plots was performed to estimate the 95% percentile confidence interval. The Levines test was performed to assess the normality and homogeneity of variance. The parameters among IPTs, adenocarcinoma, squamous cell carcinoma, and pulmonary metastases were compared with one-way analysis of variance (ANOVA) and Bonferroni post hoc tests. Student's *t*-test and the 95% confidence intervals (CIs) were used to compare perfusion parameters between malignant and benign SPNs. Independent sample *t*-test was used for comparison of parameters for IPTs with small IPTs and large IPTs. The diagnostic accuracy of the perfusion parameters in identifying SPNs was evaluated using receiver operating characteristic (ROC) curves, and the area under the curve (AUC) was calculated to evaluate the diagnostic efficacy of all perfusion parameters. AUC of 0.50–0.70 indicated a low diagnostic value; 0.71–0.90 indicated a moderate diagnostic value; ≥0.90 indicated a high diagnostic value. Two-sided P values <0.05 were considered statistically significant.

Results

Patient characteristics

Ninety-eight consecutive patients were analyzed, including

25 with IPTs (small IPTs: 11 cases with diameters of 1≤ IPTs ≤2 cm, larger IPTs: 14 cases with diameters of 2< IPTs ≤3 cm) and 73 with malignant SPNs (30 with adenocarcinoma, 27 with squamous cell carcinoma, and 16 with pulmonary metastases: metastatic adenocarcinoma from digestive tract 7 cases, liver metastases 6 cases, and breast cancer 3 cases). All patients had analyzable image sets. The patients were 59.20±3.50 years old, and 53 (54.08%) patients were male. The nodules were 2.77±0.46 cm (*Table 1*). Representative cases are shown in *Figures 1-4*. The total DLP was 516.64 mGy·cm (32.29 mGy × 16 cm), and the effective dose was 7.23 mSv based on a k-factor of 0.014.

Table 1 Characteristics of the patients

Characteristics	Values (n=98)
Age (years), mean ± SD	59.20±3.50
Sex, n (%)	
Male	53 (54.08)
Female	45 (45.92)
Nodule size (cm), mean ± SD	2.77±0.46
Types of pulmonary nodules, n (%)	
IPTs	25 (25.51)
Malignant SPNs	73 (74.49)
Squamous cell carcinoma	27 (27.55)
Adenocarcinoma	30 (30.61)
Pulmonary metastases	16 (16.33)

IPT, inflammatory pseudotumor; SD, standard deviation; SPN, solitary pulmonary nodule.

Diagnosis of IPTs and malignant SPNs using plain CT, DI-CTP, both plain CT and DI-CTP

The diagnosis of IPTs and malignant SPNs by plain CT, DI-CTP, and CT plain scan combined with DI-CTP are shown in *Table 2*. Plain CT diagnosis of IPTs and malignant SPNs has a sensitivity of 41.1%, specificity of 24%, and accuracy of 36.73%. The sensitivity, specificity, and accuracy of DI-CTP in diagnosing pulmonary nodules are 96%, 97.26%, and 96.93%, respectively. The sensitivity, specificity, and accuracy of CT plain scan combined with DI-CTP in diagnosing pulmonary nodules are 100%,

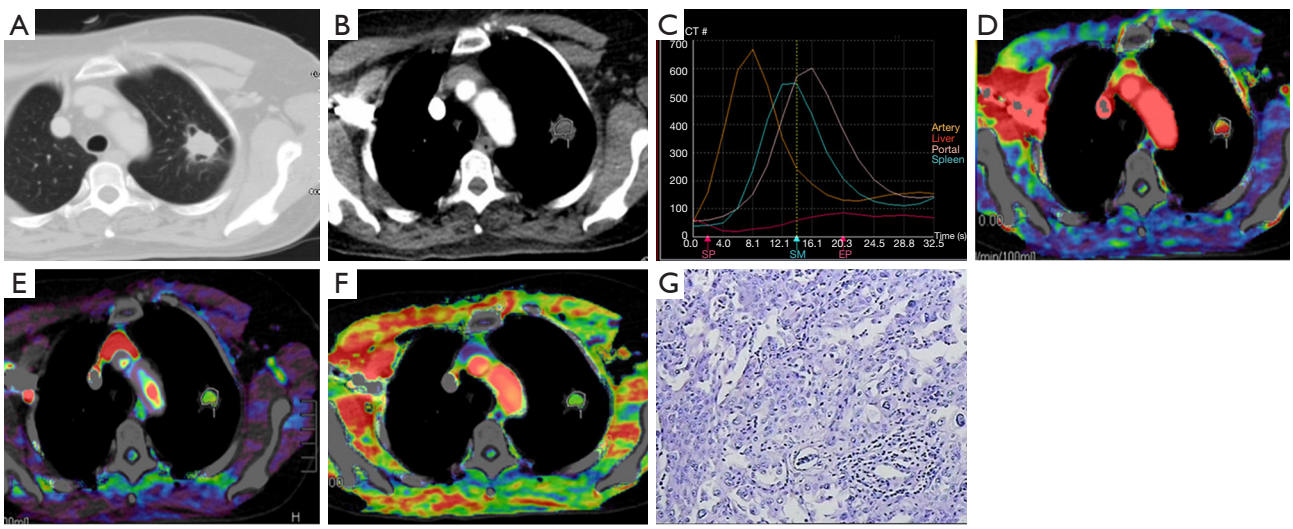

Figure 1 DI-CTP and pathology of patient with a poorly differentiated adenocarcinoma. (A-G) Axial non-contrast CT showing pulmonary lesions with varying short and length burrs in a 53-year-old female patient located in the left upper lobe (A), moderate CT enhancement (B) with a CT value of 41.4 HU in $Area_1$ (ROI). Perfusion profile: the ascending branch was steep, slightly decreased after reaching the peak, and then maintained at a high level. The first-pass TTP was 20.3 s (C), a PF of 87.0 mL/min/100 mL (D), a BF of 58.1 mL/min/100 mL (E), and a PI of 56.2% (F) in $Area_1$, pathologically confirmed as a poorly differentiated adenocarcinoma staining with hematoxylin and eosin (×400) (G). BF, bronchial artery flow; CT, computed tomography; DI-CTP, dual-input volume CT-perfusion; EP, end phase, tissue peak enhancement; HU, Hounsfield unit; PF, pulmonary artery flow; PI, perfusion index; ROI, region of interest; SM, spleen peak time; SP, start phase; TTP, time-to-peak.

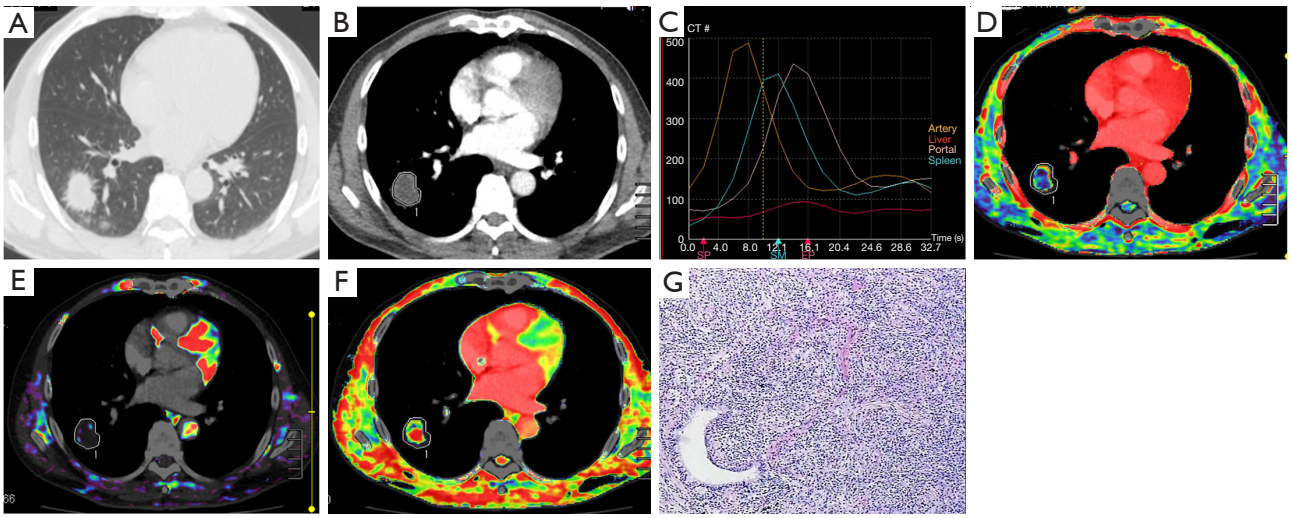

Figure 2 DI-CTP and pathology of patient with a moderately differentiated squamous cell carcinoma. (A-G) Axial non-contrast CT showing pulmonary lesions with lobulation sign in a 65-year-old male patient located in the left superior lobe (A), moderate CT enhancement with a CT value of 32.3 HU in $Area_1$ (ROI) (B). Perfusion profile: flat straight line with low amplitude enhancement peak. The first-pass TTP was 22.5 s (C), a PF of 37.7 mL/min/100 mL (D), a BF of 59.1 mL/min/100 mL (E), and a PI 35% (F) in $Area_1$. Pathologically confirmed as a moderately differentiated squamous cell carcinoma staining with hematoxylin and eosin (×40) (G). BF, bronchial artery flow; CT, computed tomography; DI-CTP, dual-input volume CT-perfusion; EP, end phase, tissue peak enhancement; HU, Hounsfield unit; PF, pulmonary artery flow; PI, perfusion index; ROI, region of interest; SM, spleen peak time; SP, start phase; TTP, time-to-peak.

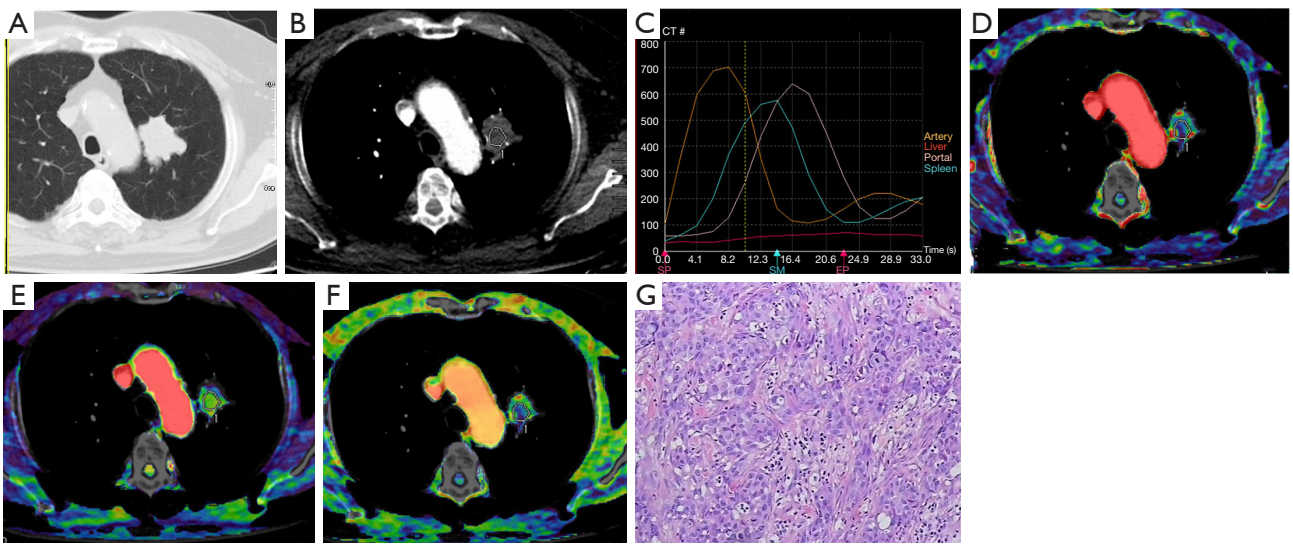

Figure 3 DI-CTP and pathology of patient with pulmonary metastasis (from the liver). (A-G) Axial non-contrast CT showing pulmonary lesions with lobulation sign in a 56-year-old female patient located in the left lower lobe (A), mild CT enhancement with a CT value of 18.5 HU in $Area_1$ (ROI) (B). Perfusion profile: the ascending branch of the curve reaches its peak value and then slowly decreases, but the density at the end of the curve is higher than that before enhancement. The first-pass TTP was 20.4 s (C), a PF of 39.3 mL/min/100 mL (D), a BF of 47.1 mL/min/100 mL (E), and a PI of 41.3% (F) in $Area_1$. Pathologically confirmed as pulmonary metastasis (from the liver) staining with hematoxylin and eosin (×400) (G). BF, bronchial artery flow; CT, computed tomography; DI-CTP, dual-input volume CT-perfusion; EP, end phase, tissue peak enhancement; HU, Hounsfield unit; PF, pulmonary artery flow; PI, perfusion index; ROI, region of interest; SM, spleen peak time; SP, start phase; TTP, time-to-peak.

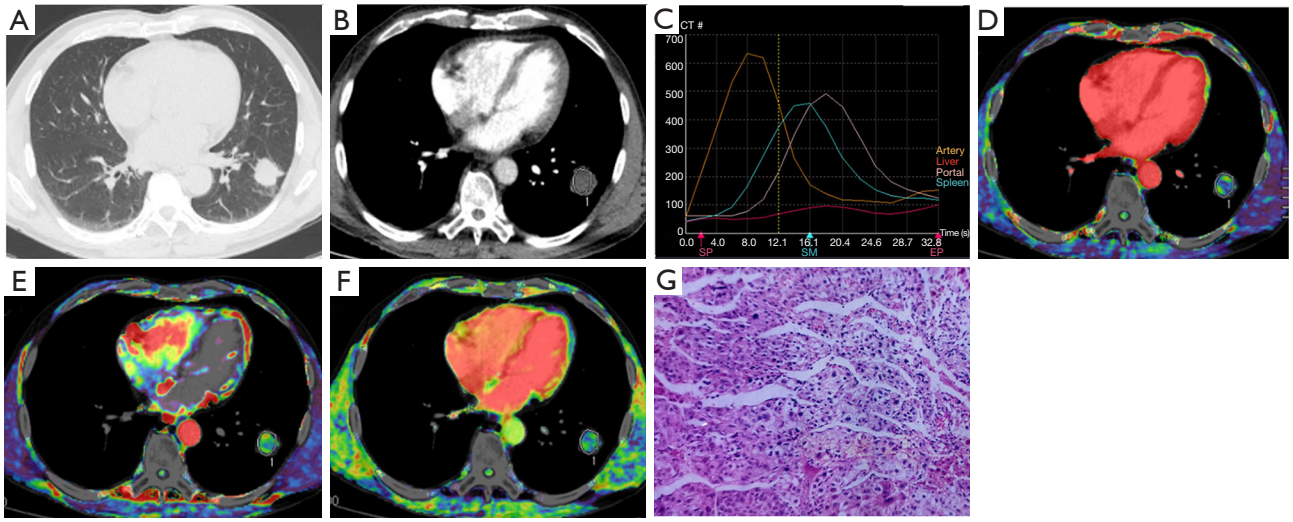

Figure 4 DI-CTP and pathology of patient with IPT. (A-G) Axial non-contrast CT showing pulmonary lesions with varying short burrs in a 53-year-old male patient located in the right inferior lower lobe (A), uneven mild CT enhancement with a CT value of 21.4 HU in $Area_1$ (ROI) (B). Perfusion profile: the ascending branch of the curve rapidly reached the peak and then declined sharply, with the density at the end of the curve returning to the same level as before enhancement. The first-pass TTP was 16.1 s (C), with a PF of 40.0 mL/min/100 mL (D), a BF of 29.1 mL/min/100 mL (E), and a PI of 38.7% (F) in $Area_1$. Pathological examination confirmed the lesion as an IPT, as demonstrated by hematoxylin and eosin staining (×400) (G). BF, bronchial artery flow; CT, computed tomography; DI-CTP, dual-input volume CT-perfusion; EP, end phase, tissue peak enhancement; HU, Hounsfield unit; IPT, inflammatory pseudotumor; PF, pulmonary artery flow; PI, perfusion index; ROI, region of interest; SM, spleen peak time; SP, start phase; TTP, time-to-peak.

Table 2 Diagnosis of IPTs and malignant SPNs using plain CT, DI-CTP, both plain CT and DI-CTP

Pathological type	Plain CT, n (%)		DI-CTP, n (%)		Both plain CT and DI-CTP, n (%)	
	IPTs	Malignant SPNs	IPTs	Malignant SPNs	IPTs	Malignant SPNs
IPTs	6 (24.0)	19 (76.0)	24 (96.0)	1 (4.0)	25 (100.0)	0
Malignant SPNs	43 (58.9)	30 (41.1)	2 (2.74)	71 (97.26)	1 (1.36)	72 (98.63)
Total	48 (48.97)	50 (51.02)	26 (26.53)	72 (73.46)	26 (26.53)	72 (73.46)

CT, computed tomography; DI-CTP, dual-input volume computed tomography perfusion; IPT, inflammatory pseudotumor; SPN, solitary pulmonary nodule.

96.83%, and 98.97%, respectively.

Reproducibility, intra/inter-observer agreement, and scattered plots of DI-CTP parameters

The Bland-Altman analysis for intra- and inter-observer agreement and assessment of patterns of PI with scattered plots showed that most of the plots of absolute difference were within the 95% limits of agreement, suggesting that the test-retest variability of the DI-CTP parameters in pulmonary nodules was acceptable in this study (Figures S1,S2).

The ICCs in the measurement of all the parameters and reproducibility coefficients (RCs) for each observer are presented in *Table 3*. The ICCs for inter-observer and intra-observer reliability of all parameters were perfect (all ICCs >0.90, P<0.01). The correlations between the two radiologists were excellent. The RCs for all parameters between the first and second measurements ranged from 0.87 to 8.03 (intra-observer agreement) and from 1.06 to 9.90 (inter-observer agreement). The CV for each index was <20%.

Table 3 Intra- and inter-observer agreement in measurement and coefficient of variation of DI-CTP parameters

Parameters	Intra-observer agreement					Inter-observer agreement				
	ICC1	f	P	RC	CV	ICC2	f	P	RC	CV
PF (mL/min/100 mL)	0.97 (0.95–0.98)	68.07	<0.01	6.22	19.19	0.95 (0.95–0.97)	44.30	<0.01	6.94	18.72
BF (mL/min/100 mL)	0.92 (0.89–0.94)	25.21	<0.01	6.05	18.87	0.93 (0.88–0.94)	25.89	<0.01	6.60	19.27
TLP (mL/min/100 mL)	0.97 (0.95–0.98)	66.11	<0.01	8.03	15.11	0.95 (0.93–0.96)	41.88	<0.01	9.90	15.04
PI (%)	0.95 (0.92–0.96)	37.96	<0.01	3.34	11.10	0.92 (0.89–0.95)	25.87	<0.01	4.02	11.72
TTP (s)	0.98 (0.97–0.98)	126.21	<0.01	0.87	13.07	0.97 (0.96–0.98)	82.46	<0.01	1.06	12.67

ICCs are mean (95% confidence interval). BF, bronchial artery flow; CV, coefficient of variation, expressed in percent; ICC, intraclass correlation coefficient; ICC1, ICC between two measurements by Observer 1; ICC2, ICC between average measurements by Observer 1 and measurements by Observer 2; PF, pulmonary artery flow; PI, perfusion index; RC, reproducibility coefficient, expressed in percent; TLP, total perfusion; TTP, time-to-peak enhancement.

Table 4 Comparison of DI-CTP parameters between malignant SPNs and IPTs

Parameters	IPTs (n=25)	Malignant SPNs (n=73)	P[#]	Adenocarcinomas (n=30)	Squamous cell carcinomas (n=27)	Pulmonary metastases (n=16)	P[&]
PF (mL/min/100 mL)	56.29±9.24	65.66±12.06**	<0.01	73.86±9.57**	57.84±9.17	67.77±11.46**	<0.01
BF (mL/min/100 mL)	44.20±8.59	47.97±8.36	0.09	50.23±7.06	48.34±11.07	45.53±5.69	0.06
TLP (mL/min/100 mL)	100.50±15.55	113.64±5.88**	<0.01	124.09±14.12**	106.25±15.03	112.30±12.05	<0.01
PI (%)	45.29±4.42	47.29±5.45	0.13	47.63±6.06	45.56±5.12	48.76±3.70*	0.08
TTP (s)	15.51±1.12	20.62±1.71**	<0.01	19.96±1.30**	19.45±1.60**	19.78±1.11**	<0.01

Data are mean ± standard deviation for PF, BF, TLP, PI, and TTP. [#], P values for IPTs *vs.* malignant SPNs; [&], P values for IPTs *vs.* adenocarcinomas *vs.* squamous cell carcinomas *vs.* and pulmonary metastases. *, P<0.05; **, P<0.01 *vs.* the IPTs. SPN, solitary pulmonary nodule; IPT, inflammatory pseudotumor; PF, pulmonary artery flow; BF, bronchial artery flow; TLP, total perfusion; PI, perfusion index; TTP, time-to-peak enhancement.

DI-CTP parameters in malignant SPNs and IPTs

The comparisons of perfusion parameters between malignant SPNs and IPTs are shown in *Table 4*. Compared with IPTs, malignant SPNs had higher PF (65.66±12.06 *vs.* 56.29±9.24 mL/min/100 mL, P<0.01; TLP: 113.64±5.88 *vs.* 100.50±15.55 mL/min/100 mL, P<0.01), and TTP (20.62±1.71 *vs.* 15.51±1.12 s, P<0.01), without significant differences in BF (P=0.09) and PI (P=0.13).

Subgroup analysis showed significant differences in PF, TLP, and TTP among patients with adenocarcinoma, squamous cell carcinoma, pulmonary metastases, and IPTs (all P<0.01) but not in BF (P=0.06) and PI (P=0.08) (*Table 4*). PF was significantly higher in adenocarcinoma and pulmonary metastases compared with IPTs (adenocarcinoma, 73.86±9.57 *vs.* 56.29±9.24 mL/min/100 mL, P<0.01; pulmonary metastases, 67.77±11.46 *vs.* 56.29±9.24 mL/min/100 mL, P<0.01). Compared with IPTs, TLP in adenocarcinoma and PI in pulmonary metastases were higher (TLP, 124.09±14.12 *vs.* 100.50±15.55 mL/min/100 mL, P<0.01; PI, 48.76%±3.70% *vs.* 45.29%±4.42%, P<0.05). TTP was lower in IPTs compared with adenocarcinoma, squamous cell carcinoma, and pulmonary metastases (adenocarcinoma, 19.96±1.30 *vs.* 15.51±1.12 s, P<0.01; squamous cell carcinoma, 19.45±1.60 *vs.* 15.51±1.12 s, P<0.01; pulmonary metastases, 19.78±1.11 *vs.* 15.51±1.12, P<0.01).

Subgroup analysis showed significant differences in PF, and TLP among patients with gastrointestinal metastatic adenocarcinoma, liver metastases, and breast metastatic cancer (all P<0.01), but not in BF (P=0.64), PI (P=0.66) or TTP(P=0.94). PF was significantly higher in gastrointestinal metastatic adenocarcinoma (72.78±10.14 mL/min/100 mL) compared with liver metastases (62.35±2.80 mL/min/100 mL, P<0.05) and

Table 5 Diagnostic performance of DI-CTP parameters in the differentiating IPTs and malignant SPNs

Parameters	AUC	Cutoff	Sensitivity (%)	Specificity (%)	PPV (%)	NPV (%)	Accuracy (%)
PF (mL/min/100 mL)	0.752	56.2	68.0	74.0	78.4	66.7	75.5
BF (mL/min/100 mL)	0.609	45.7	64.0	61.6	68.0	52.2	64.3
TLP (mL/min/100 mL)	0.728	105.2	76.0	64.4	75.6	60.0	72.5
PI (%)	0.628	46.7	76.0	56.2	71.2	40.0	63.3
TTP (s)	0.987	18.1	92.0	97.3	97.3	96.0	96.9

DI-CTP, dual-input volume computed tomography perfusion; IPT, inflammatory pseudotumor; SPN, solitary pulmonary nodule; PF, pulmonary artery flow; BF, bronchial artery flow; TLP, total perfusion; PI, perfusion index; TTP, time-to-peak; AUC, area under the curve; PPV, positive predictive value; NPV, negative predictive value.

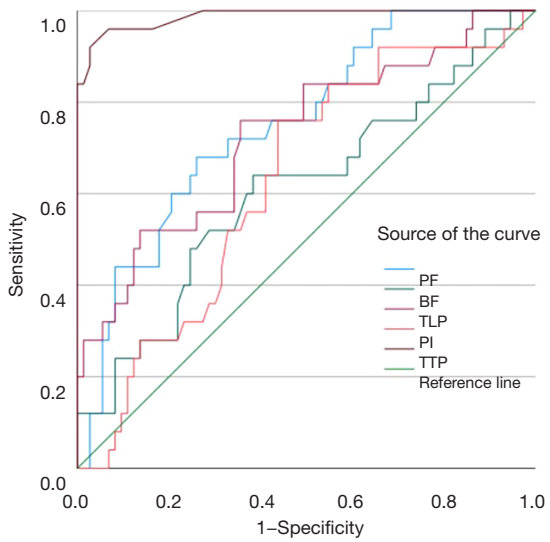

Figure 5 ROC curve analysis of the five perfusion parameters (PF, BF, PI, TLP, and TTP) for detecting malignant SPNs. BF, bronchial artery flow; PF, pulmonary artery flow; PI, perfusion index; ROC, receiver-operating characteristic; SPN, solitary pulmonary nodule; TLP, total perfusion; TTP, time-to-peak enhancement.

breast metastatic cancer (51.63±10.75 mL/min/100 mL, P<0.01). TLP was lower in breast metastatic cancer (97.30±10.43 mL/min/100 mL) compared with gastrointestinal metastatic adenocarcinoma (118.44±8.12 mL/min/100 mL, P<0.01).

Subgroup analysis showed the larger IPTs are associated with richer blood supply than the small lesions (PF, 59.51±8.66 *vs.* 50.97±7.31 mL/min/100 mL, P<0.05; BF, 48.27±8.45 *vs.* 39.94±5.86 mL/min/100 mL, P<0.05 and TLP 107.78±14.66 *vs.* 91.19±10.47 mL/min/100 mL, P<0.01).

ROC curve analysis

The diagnostic characteristics according to the threshold values are summarized in *Table 5*. Compared with other perfusion parameters (PF, BF, TLP, and PI), TTP had a larger AUC (0.987 *vs.* 0.752 *vs.* 0.609 *vs.* 0.728 *vs.* 0.628) (*Figure 5*). With a cut-off TTP of 18.10 s to distinguish IPNs from malignant SPNs, the sensitivity, specificity, positive predictive value (PPV), negative predictive value (NPV), and accuracy were 92.0%, 97.3%, 97.3%, 96.0%, and 96.9%, respectively.

Discussion

Good management of the SPNs was supposed to reduce lung cancer mortality. Differentiating malignant from benign SPNs when only conventional CT data are available is always a challenge for the radiologist because of the huge overlap in morphological findings between malignancy and benignity (1,24,25). The advent of DI-CTP with 320-row volume CT allows the immediate acquisition of isotropic volume data within a 16-cm area through continuous dynamic scanning. It has made it possible to differentiate between benign and malignant SPNs non-invasively (15,20,26). However, previous findings on DI-CTP perfusion parameters such as PF, BF, and PI in differentiating benign from malignant SPNs have been inconsistent (13,18). The TTP derived from TDC reflects the characteristics of its dominant blood supply in pulmonary nodules. Studies have demonstrated that benign SPNs have lower TTP than malignant SPNs (21,22). IPT is one of the rare benign SPNs in the lung (4,27). It is often misdiagnosed as a malignant SPN because its imaging features overlap with those of malignant SPNs, leading to overtreatment (6-9). Research on the use of TTP

to distinguish IPTs from malignant SPNs, particularly different subtypes of malignant SPNs, is currently lacking. Therefore, the present retrospective study investigated the value of first-pass TTP to distinguish IPTs from malignant SPNs using DI-CTP. The results suggested that PF, TLP, and PI were similar in IPTs, adenocarcinoma, and squamous cell carcinoma, and BF had similar values in IPTs and pulmonary metastases. These four parameters may not perform well in distinguishing IPTs from certain types of malignant SPNs. In contrast, TTP was significantly lower in IPTs compared with all three types of malignant SPNs and could be a valuable parameter for differentiating between IPTs and different types of malignant SPNs.

The comparison of intra-observer agreements for each index assessment revealed that all indexes featured excellent correlation between first and second measurements, and the RC was good enough for clinical purposes as established in previously published studies (17,28-30). This suggests that first-pass DI-CTP parameters are reproducible and applicable to routine clinical practice.

Blood supply analysis of pulmonary nodules is of great clinical significance for preoperative diagnosis of diverse pathologies, including benign and malignant nodules (16,31). The quantification of PF and BF in lung disorders has been achieved with DI-CTP analysis based on dynamic volume CT, producing helpful information for treatment planning (32), antitumor therapy (33), and embolization treatment (15). Still, the available studies showed that not all malignant lesions are mainly supplied by the bronchial artery (20,22,34). Some malignant lesions may have a dual blood supply or even be mainly supplied by the pulmonary artery. These findings were confirmed by CT imaging in human and animal studies (35). In this study, both IPTs and malignant SPNs had dual bronchial and pulmonary artery blood supply. IPTs and malignant SPNs showed significant differences in PF and TLP, but were similar in BF and PI, which were in line with previous studies (16,18,24).

TDCs represent the microvascular density of pulmonary nodules. TTP, derived from TDC, reflects the characteristics of its dominant blood supply in pulmonary nodules, which is physiologically based on dual blood supply in the lung (15,22,34). The pulmonary artery phase is earlier than the bronchial artery phase, and the peak time of the pulmonary artery is earlier than that of the bronchial artery (36). Generally, benign pulmonary lesions are mainly supplied by the pulmonary artery (34,36,37). Previous studies have shown that TTP is lower in benign SPNs than malignant SPNs (21,22). Sartori *et al.* (37) and Caremani *et al.* (34) found that after injection of ultrasound contrast agent, the arrival time (AT) of benign nodules was below 7.5 s (or 10 s), while that of malignant nodules was above 7.5 s (or 10 s). We found that TTP was significantly lower in IPTs than in all three types of malignant SPNs (adenocarcinoma, squamous cell carcinoma, and pulmonary metastases), and ROC curve analysis for diagnostic performance assessment clearly showed an AUC of 0.987 for TTP in the differential diagnosis of malignant SPNs and IPTs. With TTP =18.1 s as a cutoff, sensitivity and specificity were 92.0% and 97.3%, respectively, indicating a high diagnostic value. DI-CTP-derived TTP was longer than contrast-enhanced ultrasonography (CEUS)-derived AT. A reasonable explanation might be that TTP reflects the contrast agent accumulates at the peak time of the lesion, while AT is the time that the contrast agent reaches the lesion.

Regarding the radiation dosage, this study used 320-row volume CT with a tube voltage of 100 kV and a tube current of 30 mA (5.16 mSv). Therefore, the present study, as well as previous studies (15,16,18,20,38), showed that first-pass DI-CTP obtained by 320-row CT significantly reduced radiation dose in comparison with conventional contrast-enhanced CT and CTP (39-41). Meanwhile, DI-CTP is based on the maximum slope method and requires a high contrast injection flow rate (15). In this study, a flow rate of 6 mL/s was used, requiring only 30–50 mL of the contrast agent, which reduces contrast agent usage and related adverse reactions.

In addition, the present study had several limitations. Firstly, to reduce the influence of partial volume effects, GGNs or subsolid nodules <1 cm were not included. Secondly, only IPTs were included, and the findings should be confirmed in other benign lesions, as well as in other rare malignant lesions. Thirdly, this study did not compare the performance of other imaging tests for the diagnosis of benign and malignant SPNs, such as magnetic resonance imaging, positron emission tomography-CT, dynamic CT enhancement, etc. Fourthly, the morphological characteristics of SPNs, including nodule size and volume, could not be analyzed because of the small sample size.

Conclusions

In conclusion, because of excellent diagnostic capability, first-pass enhanced TTP obtained from DI-CTP with 320-row volume CT is better for differential diagnosis of IPTs and malignant SPNs. This may help to avoid excessive

lung biopsy, especially for IPTs.

Acknowledgments

The authors acknowledge the help of Le Zhang, a radiologist who participated in data collection; and Yang Bo, who provided the conceptualization.

Footnote

Reporting Checklist: The authors have completed the STARD reporting checklist. Available at https://qims.amegroups.com/article/view/10.21037/qims-24-1261/rc

Funding: This study was funded by the Medical Project of Hebei Province (Nos. 20221908 and 20240503) and Central Theater Command of Chinese People's Liberation Army (Nos. 2023LC06 and 2024LC08).

Conflicts of Interest: All authors have completed the ICMJE uniform disclosure form (available at https://qims.amegroups.com/article/view/10.21037/qims-24-1261/coif). The authors have no conflicts of interest to declare.

Ethical Statement: The authors are accountable for all aspects of the work in ensuring that questions related to the accuracy or integrity of any part of the work are appropriately investigated and resolved. The study was conducted in accordance with the Declaration of Helsinki (as revised in 2013) and was approved by the ethics committee of No. 82 Group Hospital of Chinese People's Liberation Army (No. 2021011). The requirement of informed consent was waived due to the retrospective nature of the study.

References

1. Yang D, Liu Y, Bai C, Wang X, Powell CA. Epidemiology of lung cancer and lung cancer screening programs in China and the United States. Cancer Lett 2020;468:82-7.
2. Xia C, Dong X, Li H, Cao M, Sun D, He S, Yang F, Yan X, Zhang S, Li N, Chen W. Cancer statistics in China and United States, 2022: profiles, trends, and determinants. Chin Med J (Engl) 2022;135:584-90.
3. Zhang Z, Zhang C, Wu P, Ruan C, Zheng L, Zhang W, Li J, Wu Y, Cai P. Comparison of enhanced thin CT sections with pathologic findings in pulmonary carcinoma, inflammatory, pseudo-tumor and pulmonary tuberculoma. Zhonghua Zhong Liu Za Zhi 2002;24:173-7.
4. Al-Obaidi A, Buess C, Mogire J, Reddy PS. Inflammatory Myofibroblastic Tumor of the Lung: An Extremely Rare Condition in Adults. Cureus 2019;11:e6432.
5. Seip T, Calderón Novoa F, Valeo Chulvi MP, Smith D, Dietrich A. IgG4 inflammatory pseudotumor mimicking primary lung cancer. Rev Fac Cien Med Univ Nac Cordoba 2023;80:66-9.
6. Li CR, Li YZ, Li YM, Zheng YS. Dynamic and contrast enhanced CT imaging of lung carcinoma, pulmonary tuberculoma, and inflammatory pseudotumor. Eur Rev Med Pharmacol Sci 2017;21:1588-92.
7. Zheng S, Shu J, Xue J, Ying C. CT Signs and Differential Diagnosis of Peripheral Lung Cancer and Inflammatory Pseudotumor: A Meta-Analysis. J Healthc Eng 2022;2022:3547070.
8. Wang XL, Shan W. Application of dynamic CT to identify lung cancer, pulmonary tuberculosis, and pulmonary inflammatory pseudotumor. Eur Rev Med Pharmacol Sci 2017;21:4804-9.
9. Gong JW, Zhang Z, Luo TY, Huang XT, Zhu CN, Lv JW, Li Q. Combined model of radiomics, clinical, and imaging features for differentiating focal pneumonia-like lung cancer from pulmonary inflammatory lesions: an exploratory study. BMC Med Imaging 2022;22:98.
10. Zhang M, Kono M. Solitary pulmonary nodules: evaluation of blood flow patterns with dynamic CT. Radiology 1997;205:471-8.
11. Narla LD, Newman B, Spottswood SS, Narla S, Kolli R. Inflammatory pseudotumor. Radiographics 2003;23:719-29.
12. Baratella E, Cernic S, Minelli P, Furlan G, Crimì F, Rocco S, Ruaro B, Cova MA. Accuracy of CT-Guided Core-Needle Biopsy in Diagnosis of Thoracic Lesions Suspicious for Primitive Malignancy of the Lung: A Five-Year Retrospective Analysis. Tomography 2022;8:2828-38.
13. Yuan X, Zhang J, Quan C, Cao J, Ao G, Tian Y, Li H. Differentiation of malignant and benign pulmonary nodules with first-pass dual-input perfusion CT. Eur

Radiol 2013;23:2469-74.
14. Milne EN. Circulation of primary and metastatic pulmonary neoplasms. A postmortem microarteriographic study. Am J Roentgenol Radium Ther Nucl Med 1967;100:603-19.
15. Yuan X, Zhang J, Ao G, Quan C, Tian Y, Li H. Lung cancer perfusion: can we measure pulmonary and bronchial circulation simultaneously? Eur Radiol 2012;22:1665-71.
16. Ohno Y, Fujisawa Y, Koyama H, Kishida Y, Seki S, Sugihara N, Yoshikawa T. Dynamic contrast-enhanced perfusion area-detector CT assessed with various mathematical models: Its capability for therapeutic outcome prediction for non-small cell lung cancer patients with chemoradiotherapy as compared with that of FDG-PET/CT. Eur J Radiol 2017;86:83-91.
17. Ohno Y, Koyama H, Matsumoto K, Onishi Y, Takenaka D, Fujisawa Y, Yoshikawa T, Konishi M, Maniwa Y, Nishimura Y, Ito T, Sugimura K. Differentiation of malignant and benign pulmonary nodules with quantitative first-pass 320-detector row perfusion CT versus FDG PET/CT. Radiology 2011;258:599-609.
18. Bohlsen D, Talakic E, Fritz GA, Quehenberger F, Tillich M, Schoellnast H. First pass dual input volume CT-perfusion of lung lesions: The influence of the CT- value range settings on the perfusion values of benign and malignant entities. Eur J Radiol 2016;85:1109-14.
19. Eldridge L, Moldobaeva A, Zhong Q, Jenkins J, Snyder M, Brown RH, Mitzner W, Wagner EM. Bronchial Artery Angiogenesis Drives Lung Tumor Growth. Cancer Res 2016;76:5962-9.
20. Nguyen-Kim TD, Frauenfelder T, Strobel K, Veit-Haibach P, Huellner MW. Assessment of bronchial and pulmonary blood supply in non-small cell lung cancer subtypes using computed tomography perfusion. Invest Radiol 2015;50:179-86.
21. Li Y, Yang ZG, Chen TW, Yu JQ, Sun JY, Chen HJ. First-pass perfusion imaging of solitary pulmonary nodules with 64-detector row CT: comparison of perfusion parameters of malignant and benign lesions. Br J Radiol 2010;83:785-90.
22. Hong-Xia Z, Wen H, Ling-Gang C, Wen-Jia C, Shuo L, Li-Juan D, Hai-Man S, Yang Z. A New Method for Discriminating between Bronchial and Pulmonary Arterial Phases using Contrast-Enhanced Ultrasound. Ultrasound Med Biol 2016;42:1441-9.
23. Jelliffe RW, Schumitzky A, Bayard D, Fu X, Neely M. Describing Assay Precision-Reciprocal of Variance Is Correct, Not CV Percent: Its Use Should Significantly Improve Laboratory Performance. Ther Drug Monit 2015;37:389-94.
24. Zou M, Zhao Z, Zhang B, Mao H, Huang Y, Wang C. Pulmonary lesions: correlative study of dynamic triple-phase enhanced CT perfusion imaging with tumor angiogenesis and vascular endothelial growth factor expression. BMC Med Imaging 2021;21:158.
25. Ohno Y, Fujisawa Y, Yui M, Takenaka D, Koyama H, Sugihara N, Yoshikawa T. Solitary pulmonary nodule: Comparison of quantitative capability for differentiation and management among dynamic CE-perfusion MRI at 3 T system, dynamic CE-perfusion ADCT and FDG-PET/CT. Eur J Radiol 2019;115:22-30.
26. Wang Q, Zhang Z, Shan F, Shi Y, Xing W, Shi L, Zhang X. Intra-observer and inter-observer agreements for the measurement of dual-input whole tumor computed tomography perfusion in patients with lung cancer: Influences of the size and inner-air density of tumors. Thorac Cancer 2017;8:427-35.
27. Liu C, Ma C, Duan J, Qiu Q, Guo Y, Zhang Z, Yin Y. Using CT texture analysis to differentiate between peripheral lung cancer and pulmonary inflammatory pseudotumor. BMC Med Imaging 2020;20:75.
28. Ohno Y, Koyama H, Fujisawa Y, Yoshikawa T, Seki S, Sugihara N, Sugimura K. Dynamic contrast-enhanced perfusion area detector CT for non-small cell lung cancer patients: Influence of mathematical models on early prediction capabilities for treatment response and recurrence after chemoradiotherapy. Eur J Radiol 2016;85:176-86.
29. Ohno Y, Nishio M, Koyama H, Seki S, Tsubakimoto M, Fujisawa Y, Yoshikawa T, Matsumoto S, Sugimura K. Solitary pulmonary nodules: Comparison of dynamic first-pass contrast-enhanced perfusion area-detector CT, dynamic first-pass contrast-enhanced MR imaging, and FDG PET/CT. Radiology 2015;274:563-75.
30. Ng CS, Chandler AG, Wei W, Anderson EF, Herron DH, Charnsangavej C, Kurzrock R. Reproducibility of perfusion parameters obtained from perfusion CT in lung tumors. AJR Am J Roentgenol 2011;197:113-21.
31. Lee SM, Lee HJ, Kim JI, Kang MJ, Goo JM, Park CM, Im JG. Adaptive 4D volume perfusion CT of lung cancer: effects of computerized motion correction and the range of volume coverage on measurement reproducibility. AJR Am J Roentgenol 2013;200:W603-9.
32. Li XS, Fan HX, Fang H, Huang H, Song YL, Zhou CW. Value of whole-tumor dual-input perfusion CT in predicting the effect of multiarterial infusion

chemotherapy on advanced non-small cell lung cancer. AJR Am J Roentgenol 2014;203:W497-505.
33. Yabuuchi H, Kawanami S, Iwama E, Okamoto I, Kamitani T, Sagiyama K, Yamasaki Y, Honda H. Prediction of Therapeutic Effect of Chemotherapy for NSCLC Using Dual-Input Perfusion CT Analysis: Comparison among Bevacizumab Treatment, Two-Agent Platinum-based Therapy without Bevacizumab, and Other Non-Bevacizumab Treatment Groups. Radiology 2018;286:685-95.
34. Caremani M, Benci A, Lapini L, Tacconi D, Caremani A, Ciccotosto C, Magnolfi AL. Contrast enhanced ultrasonography (CEUS) in peripheral lung lesions: A study of 60 cases. J Ultrasound 2008;11:89-96.
35. Cheng Z, Wang Y, Yuan M, Liang J, Feng Y, Shi Y, Zhang Z, Shan F. CT perfusion imaging can detect residual lung tumor early after radiofrequency ablation: a preliminary animal study on both tumoral and peri-tumoral region assessment. J Thorac Dis 2022;14:64-75.
36. Bi K, Zhou RR, Zhang Y, Shen MJ, Chen HW, Cong Y, Zhu HM, Tang CH, Yuan J, Wang Y. US Contrast Agent Arrival Time Difference Ratio for Benign versus Malignant Subpleural Pulmonary Lesions. Radiology 2021;301:200-10.
37. Sartori S, Postorivo S, Vece FD, Ermili F, Tassinari D, Tombesi P. Contrast-enhanced ultrasonography in peripheral lung consolidations: What's its actual role? World J Radiol 2013;5:372-80.
38. Sun Y, Yang M, Mao D, Lv F, Yin Y, Li M, Hua Y. Low-dose volume perfusion computed tomography (VPCT) for diagnosis of solitary pulmonary nodules. Eur J Radiol 2016;85:1208-18.
39. Fraioli F, Anzidei M, Serra G, Liberali S, Fiorelli A, Zaccagna F, Longo F, Anile M, Catalano C. Whole-tumour CT-perfusion of unresectable lung cancer for the monitoring of anti-angiogenetic chemotherapy effects. Br J Radiol 2013;86:20120174.
40. Moon JW, Yi CA, Lee KS, Woo SY, Kwon OJ, Yang E, Kim JH, Han J. Preoperative Helical Dynamic Enhanced Multidetector Row Computed Tomography: Can It Be a Prognostic Indicator in Early-Stage Non-small Cell Lung Cancer? J Comput Assist Tomogr 2022;46:308-14.
41. Yan G, Li H, Fan X, Deng J, Yan J, Qiao F, Yan G, Liu T, Chen J, Wang L, Yang Y, Li Y, Zhao L, Bhetuwal A, McClure MA, Li N, Peng C. Multimodality CT imaging contributes to improving the diagnostic accuracy of solitary pulmonary nodules: a multi-institutional and prospective study. Radiol Oncol 2023;57:20-34.

Cite this article as: Guo C, Zhang X, Shen S, Chen W, Wang X, Zhao L, Han S. Differentiation of inflammatory pseudotumors and malignant pulmonary nodules using the time-to-peak in first-pass dual-input volume computed tomography-perfusion. Quant Imaging Med Surg 2025;15(4):2754-2765. doi: 10.21037/qims-24-1261

